PCCP
Physical Chemistry Chemical Physics

Accepted Manuscript

This article can be cited before page numbers have been issued, to do this please use: S. Guo, Y. Zhu, H. Zhao and C. Zhou, *Phys. Chem. Chem. Phys.*, 2022, DOI: 10.1039/D2CP02164A.

ROYAL SOCIETY OF CHEMISTRY

rsc.li/pccp

DOI: 10.1039/D2CP02164A

Ab initio kinetics study on 2-methyl-2-butanol oxidation induced by ȮH radicals†

Shuyan Guo‡ [a], Yuxiang Zhu‡ [b], Hao Zhao *[a], Chong-Wen Zhou *[b,c]

[a.] *College of Engineering, Peking University, Beijing 100871, PR China.*

[b.] *School of Energy and Power Engineering, Beihang University, Beijing 100191, PR China.*

[c] *Combustion Chemistry Centre, School of Biological and Chemical Science, Ryan Institute, University of Galway, Galway H91TK33, Ireland*

† Electronic Supplementary Information (ESI) available: The calculated rate coefficients and thermochemistry data.

‡ Both authors contribute equally to this work.

* Correspondence authors: h.zhao@pku.edu.cn (H. Zhao), cwzhou@buaa.edu.cn (C.-W. Zhou)

Abstract

High-level ab initio calculations were performed to investigate the kinetics of the important initial steps of 2-methyl-2-butanol (2M2B) oxidation. Hydrogen-atom abstraction reactions by hydroxyl (ȮH) radical, dehydration reactions of 2M2B molecule, and unimolecular isomerization and decomposition reactions of 2M2B radicals produced by H-atom abstraction have all been included in this work. The potential energy surfaces were characterized at the QCISD(T)/CBS//M06-2X/6-311++G(d,p) level of theory. Variational transition state theory (VTST) was employed to calculate the rate coefficients for the H-atom abstraction reactions. It is interesting to note that, the hydrogen bond formed in the transition state (TS) in H-atom abstraction reactions, leading to a ring-shaped structure, has a large influence on the electronic energy barriers and rotational-vibrational properties of the TS and thus the rate coefficients. For comparison, rate coefficient calculations have been carried out for the same reaction channel by employing different types of TS structures separately, with or without the hydrogen bond. For all unimolecular reactions studied here, pressure-dependent rate coefficients were obtained through Rice-Ramsperger-Kassel-Marcus/master equation (RRKM/ME) calculations, at pressures of 0.01–100 atm. In addition, thermochemical properties at temperatures from 300–3000 K for all species in the title reactions were calculated, which were found to be in good agreement with literature data. The kinetics and thermochemistry data calculated in this study are important in predicting the combustion properties of 2M2B, which can be used in the combustion kinetic model development of 2M2B oxidation.

Keywords: 2-Methyl-2-butanol; Hydrogen abstraction; Kinetics; Hydrogen bond interaction

View Article Online
DOI: 10.1039/D2CP02164A

1. Introduction

Combustion has long served as an important source of energy for human society. However, fossil fuels which are predominantly used are not sustainable due to their limited reserves, and are also not eco-friendly. There is increasing focus on using alcohol fuels, which can be sustainably produced from biomass and are demonstrated to have favourable combustion properties as potential alternative fuels or as additives to conventional fuels[1]. Experimental and modeling studies have been performed extensively to explore the combustion chemistry of alcohols. Sarathy et al.[2] provided a comprehensive review of alcohol combustion chemistry and it can be seen that the published studies of the oxidation of alcoholic species in the past decade mainly focused on alcohols from C_1 to C_4. However, the superiority of pentanol molecules as alternative fuels for internal combustion engines over smaller alcohol molecules was demonstrated.[2] For example, pentanols have higher carbon and hydrogen contents and thus higher LHVs similar to gasoline. They also have higher boiling points and thus have less impact on the fuel distillation curve as additives; they have a lower specific latent heat of vaporization and therefore they are easier to ignite at cold-start operating conditions, etc. The feasibility of the pentanol isomers as alternative fuels has been demonstrated by motor-scale experiments, e.g., a HCCI engine test conducted by Yang et al.[3] In addition, Lapuerta et al.[4] found that short-chain alcohols exhibit poor blending stability and low viscosity. Compared to alcohols from C_1 to C_4, pentanol is more suitable to be blended with diesel fuel. Some other studies found that a higher *n*-pentanol ratio can reduce the natural luminosity of spray combustion and lead to simultaneous reduction of NO_x[5] and soot emissions,[6] and improved thermal efficiency. Efficient production routes for pentanol isomers, for example through engineered microorganisms[7], have been explored.

To understand the combustion reaction mechanism of pentanol isomers, a number of experimental and modeling studies have been carried out. A recent review by Cai et al.[8] focused on the combustion kinetics of higher linear alcohols where the experimental studies for, mainly *n*-pentanol, were summarized, and connections between the combustion behaviours observed from combustion experiments with the combustion kinetics governed by chain length and functional groups of higher alcohols were discussed in detail. Earlier in the last decade, Heufer et al.[9] developed a kinetic model for 1-pentanol based on the previously proposed rate rules for *n*-butanol and used measured auto-ignition and speciation data to validate their model. Dagaut and co-workers employed jet-stirred reactors (JSR) to study the oxidation mechanisms of a series of pentanol isomers, including 1-pentanol,[10] 2-methyl-1-butanol[11] and 3-methyl-1-butanol[12]. More recently, Köhler et al.[13] systematically investigated the oxidation pathways of *n*-pentanol in laminar, flat, low-pressure $H_2/O_2/Ar$ based flames doped with equal amounts of pre-vaporized alcohols. Cao et al.[14] studied the pyrolysis of *n*-pentanol and 2-methyl-1-butanol in a flow reactor and developed a kinetic model to validate against their measurements. Experimental and modeling efforts have been devoted comprehensively to understanding the oxidation mechanisms of *n*-pentanol and 2-methyl-1-butanol in recent years, whereas investigations on 2-methyl-2-butanol combustion are quite limited in the literature.[15, 16] 2-methyl-2-butanol is the only tertiary pentanol isomer, and study on the kinetics of 2-methyl-2-butanol oxidation will be helpful to understanding the combustion chemistry of higher *tert*-amyl alcohols and eventually beneficial for choosing the pentanol isomer with correct isomeric properties.

H-atom abstraction, dehydration reactions of alcohol molecules, and subsequent isomerization and decomposition reactions of alcohol radicals are important initial steps among the ~30 reaction classes of alcohol oxidation.[2] Zhao et al.[17] carried out ab initio calculations for the thermal decomposition of 1-pentanol, 2-methyl-1-butanol and 3-methyl-1-butanol at the CBS-QB3 level and obtained the pressure-

dependent rate coefficients from the solutions of master equation. Aazaad et al.[18] calculated the rate coefficients at temperatures from 270–350 K for the α H-atom abstraction reactions of *n*-pentanol isomers by ȮH radicals using VTST. Van de Vijver et al.[19] studied the potential energy surfaces for the decomposition and isomerization reactions of 1-pentanol radicals at the UCCSD(T)-F12a/cc-pVTZ-F12//M06-2X/6-311++G(d,p) level of theory, and calculated the rate coefficients by solving the master equation. Xing et al.[20] implemented multi-path variational transition state theory (MP-VTST) to calculate the rate coefficients of H-atom abstraction of 3-methyl-1-butanol by ȮH radicals. Bai et al.[21] investigated the kinetics of decomposition and isomerization reactions of 2-pentanol-2-yl radical at the ROCCSD(T)/CBS//B2PLYPD3/6-311++G(d,p) level of theory, and calculated the thermochemistry properties of the important species involved in the reaction process. Bai et al.[22] studied the energetics of the H-atom abstraction reactions of 1-pentanol, 2-pentanol, and 3-pentanol by hydroxyl radicals at the CCSD(T)/CBS//M06-2X/6-311+G(d,p) level and calculated the rate coefficients by using the multi-structural variational transition state theory (MS-VTST) together with the small curvature tunnelling (SCT) correction. To date, the kinetics of the initial oxidation steps of 2-methyl-2-butanol have not been investigated either experimentally or theoretically.

In this study, the kinetics of the important primary oxidation steps of 2-methyl-2-butanol (2M2B), including hydrogen-atom abstraction reactions by hydroxyl (ȮH) radical, dehydration reactions of 2M2B, and the isomerization and β-scission reactions of 2M2B radicals were investigated theoretically. In addition, the thermochemical properties of all species involved were also calculated. This study aims to provide accurate kinetics and thermochemistry data for the important reaction classes of 2M2B oxidation which can be used in the model development for 2M2B oxidation.

2. Computational method

2.1. Potential energy surfaces

The molecular structures of all species and transition states (TS) involved in the title reactions were optimized using the M06-2X[23] method with 6-311++G(d,p)[24] basis set. The frequencies of all normal vibrational modes and the zero-point energy (ZPE) corrections were obtained at the same level of theory. Intrinsic reaction coordinate (IRC) calculations were also carried out at the M06-2X/6-311++G(d,p) level, in order to confirm that each TS connects the desired reactants and products, and to obtain the molecular properties of a number of transition structures along the reaction coordinate for the reactions with a loose TS. The one-dimensional hindered rotor approximation was applied for the low-frequency torsional modes of all species and TSs, with their hindrance potentials scanned at the M06-2X/6-31G level of theory. Single-point energies for all stationary points on the potential energy surfaces (PES) were calculated by using the quadratic configuration interaction method with singles, doubles and perturbative inclusion of triples, QCISD(T),[25] with Dunning's cc-PVDZ,[26] cc- pVTZ[27] basis sets, and the MP2[28] method with the cc-pVDZ,[26] cc-pVTZ[27] and cc-pVQZ[29] basis sets. Then the QCISD(T) and MP2 energies were extrapolated to the complete basis set (CBS) limit via the expressions:[30]

$$E_{\mathrm{QCISD(T)/CBS,\ DZ\rightarrow TZ}} = E_{\mathrm{QCISD(T)/TZ}} + (E_{\mathrm{QCISD(T)/TZ}} - E_{\mathrm{QCISD(T)/DZ}}) \times 0.4629 \quad (1)$$

$$E_{\mathrm{MP2/CBS,\ TZ\rightarrow QZ}} = E_{\mathrm{MP2/QZ}} + (E_{\mathrm{MP2/QZ}} - E_{\mathrm{MP2/TZ}}) \times 0.6938 \quad (2)$$

$$E_{\mathrm{MP2/CBS,\ DZ\rightarrow TZ}} = E_{\mathrm{MP2/TZ}} + (E_{\mathrm{MP2/TZ}} - E_{\mathrm{MP2/DZ}}) \times 0.4629 \quad (3)$$

$$E_{\mathrm{QCISD(T)/CBS}} = E_{\mathrm{QCISD(T)/CBS,\ DZ\rightarrow TZ}} + E_{\mathrm{MP2/CBS,\ TZ\rightarrow QZ}} - E_{\mathrm{MP2/CBS,\ DZ\rightarrow TZ}} \quad (4)$$

The electronic structure and single point energy calculations in this study were performed by using the Molpro 2015[31] program.

2.2. Rate coefficient calculations

In this study, variational transition state theory (VTST) was employed to calculate the rate coefficients for the H-atom abstraction reactions by ȮH radicals, because of their relatively small energy barriers of ~1.5 kcal mol^{-1} or submerged TSs below the reactants in energy. The Hessians of the transition structures along the minimum energy path obtained from IRC calculations were employed to calculate the normal mode vibrational frequencies and the ZPEs using the ProjRot code from the Auto-Mech program suite.[32] On the other hand, the reaction kinetics of dehydration reactions of 2M2B, and isomerization and decomposition reactions of 2M2B radicals were explored by performing the Rice-Ramsperger-Kassel-Marcus/master equation (RRKM/ME) calculations, in order to obtain pressure-dependent rate coefficients in the pressure range 0.01–100 atm with N_2 as the bath gas. For all reactions investigated in this study, the Master Equation System Solver (MESS)[33] program was used to calculate the rate coefficients, with rigid-rotor-harmonic-oscillator (RRHO) model employed to characterize the rotational-vibrational degrees of freedom while 1-D hindered rotor approximation was applied for the torsional modes. Asymmetric Eckart model[34] was applied to quantify the tunnelling effects. In the master equation modeling, the collisional frequency was modeled by using the Lennard-Jones (L-J) potential[35], with the parameters σ = 3.6 Å, ε = 68 cm^{-1} for N_2 and σ = 6.27 Å, ε = 341.3 cm^{-1} employed for another $C_5H_{11}O$ system[21] adopted here for the 2M2B and 2M2B radicals by analogy. The exponential-down model[36] was employed to describe collisional energy relaxation, with average downward energy transferred per collision estimated as $\langle\Delta E_{down}\rangle = 200 \times (T/300)^{0.75}$ cm^{-1}.[21] The calculated phenomenological rate coefficients for title reactions were fitted by modified Arrhenius expression and provided in the ESI†.

2.3. Thermochemistry calculations

The molecular partition functions calculated by using the MESS[33] code were employed to compute the temperature-dependent enthalpies (H), entropies (S) and heat capacities (C_p) for all species involved in the title reactions via calls to the ThermP[37] code. The enthalpies of formation at 0 K for all species were calculated based on atomization approach, by using CBS-APNO,[38] CBS-QB3,[39] G3,[40] and G4[41] composite methods and taking the average, which showed good agreement (rivalling "chemical accuracy", 1 kcal/mol) with the ATcT benchmarked formation enthalpies for some 50 $C_xH_yO_z$ molecules.[42] The calculated thermochemistry properties at temperatures from 300 to 3000 K were finally fitted by NASA polynomial through PAC99[43] program, and provided in the ESI†.

View Article Online
DOI: 10.1039/D2CP02164A

3. Results and discussion

3.1. H-atom abstraction reactions by ȮH radicals

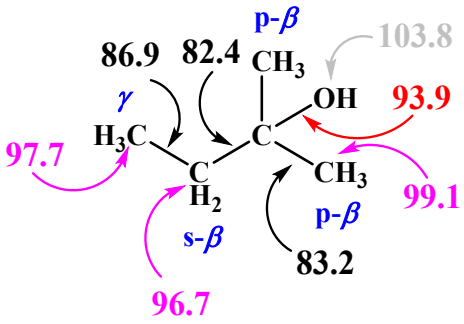

Fig. 1 Definitions of different carbon sites on 2-methyl-2-butanol (2M2B) with "p-β" denotes primary beta site and "s-β" denotes secondary beta site, and bond dissociation energies at 0 K (kcal/mol) calculated at the G4[41] level of theory.

As illustrated in Fig. 1, relative to the hydroxyl group 2M2B molecule has two primary β sites (p-β), one secondary β (s-β) site and one γ site, from which a hydrogen atom can be abstracted and four different radicals, namely, 2-methyl-2-butoxy, 2M2B-1-yl, 2M2B-3-yl and 2M2B-4-yl can be produced. The bond dissociation energy (BDE) for the C–H bond at the s-β site is the lowest, while the BDE for the O–H bond is ~5 kcal/mol higher than those for the C–H bonds. It is important to note that, except for the TS of H-atom abstraction reaction from the hydroxyl group, a hydrogen bond could be formed between the hydroxyl group and ȮH radical in the TSs of the other three H-atom abstraction reaction pathways by ȮH radical, leading to a ring-shaped structure. As discussed by Rotavera and Taatjes[44], the effects of hydrogen bonding in TSs lead to differences in rate coefficients and branching fractions of the initiation oxidation steps, which could have pronounced influence on the combustion kinetics of oxygenated species at lower temperatures. Transition state geometries with and without hydrogen bond for the same position is shown in Table 1 and the hydrogen bonds are typically ~2.0 Å which will lower the electronic energy barrier. With different geometries, partition functions for the TSs with or without hydrogen bond, calculated with the RRHO treatment for the rotational and vibrational degrees of freedom and 1-D hindered rotor descriptions for the internal torsional modes, are also quite different. Moreover, since the formation of a ring converts the internal rotational degrees of freedom to ring vibrations, and eventually leads to lower entropy[45], it is considered less favored under combustion temperature regimes. In order to investigate the effect of hydrogen bond formed in the TS on reaction kinetics, rate coefficients for the H-atom abstraction reactions from the p-β, s-β and γ sites were calculated by using the TS structures with and without hydrogen bond shown in Table 1 separately. Different electronic energy barriers and rotational-vibrational properties corresponding to the different TS geometries were used in the rate constants calculations for comparison.

Table 1. Saddle point geometries employed for H-atom abstraction reactions from the carbon sites, obtained at the M06-2X/6-311++G(d,p) level of theory (with atomic distances in units of Å).

With hydrogen bond	Without hydrogen bond

View Article Online
DOI: 10.1039/D2CP02164A

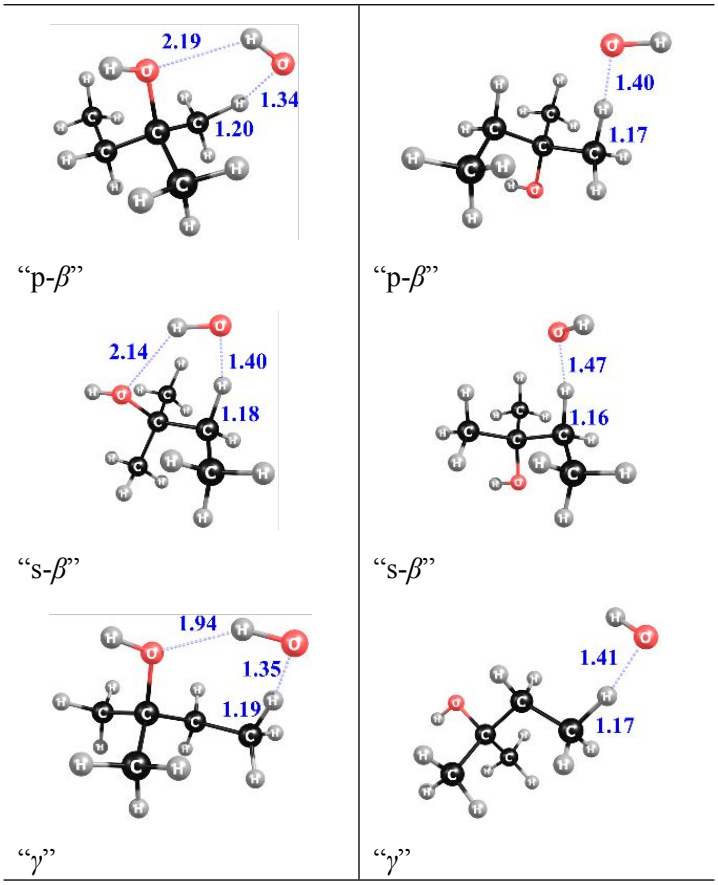

The relative electronic energies to the reactants, 2M2B + ȮH, for all stationary points on the PESs of the H-atom abstraction reactions are shown in Fig. 2. A pre-reaction van der Waals complex was located for each reaction channel. The reactants will undergo a barrier-less reaction channel to form the van der Waals complex, and then surmount the inner TS barrier to finally become the bimolecular products. Since the bottleneck of reactive fluxes is at the inner TS and the kinetic effect of the barrier-less entrance reaction channel is negligible at temperatures above 300 K,[46, 47] a one-TS model including only the inner TS is expected to be sufficient for the rate coefficient calculations here. The energy differences between the inner TS, and the van der Waals complex and products respectively, were employed as well depths in Eckart tunnelling model. In general, the electronic energies of TSs for all H-atom abstraction reactions of 2M2B by ȮH are quite close to those of the reactants and are even lower, indicating the necessity of the variational correction. The s-β H-atom abstraction reaction channel has the lowest energy barrier of –2.0 kcal mol^{-1}, while the H-atom abstraction reaction from the hydroxyl group has the highest energy barrier of 1.6 kcal mol^{-1}, and the energy barriers for the p-β and γ H-atom abstraction reactions lie in between. The TS conformers with hydrogen bond stay lower in energy than those without hydrogen bond by 1.5–3.0 kcal mol^{-1}, which is attributed to the stabilization effect of the formation of hydrogen bond. In addition, the effect of hydrogen bond on the torsional and vibrational modes of the TS is also observed. Being locked by the hydrogen bond, the rotational energy barriers of the C–C and C–O typically increase by 5 kcal mol^{-1} or larger, e.g., Fig. 3, which decreases their contributions to the overall TS partition function. Moreover, the vibrational degrees of freedom of the TS will also be affected by the ring strain. For example, Table 2 shows the calculated normal mode vibrational frequencies of the two different types of TS conformers for the H-atom abstraction reaction from the s-β site. The vibrational frequencies below 1000 cm^{-1} become higher with the presence of

View Article Online
DOI: 10.1039/D2CP02164A

hydrogen bond. With harmonic oscillator approximation implemented for the normal modes, the vibrational partition functions for the TS will decrease when frequencies increase.

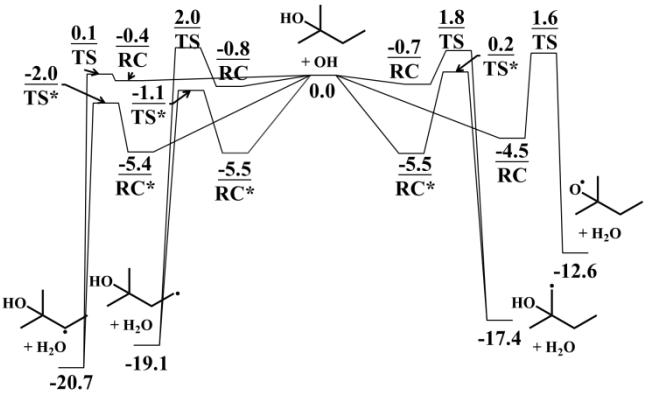

Fig. 2 ZPE corrected PESs (in units of kcal mol^{-1}) for the H-atom abstraction reactions from 2M2B by ȮH at the QCISD(T)/CBS//M06-2X/6-311++G(d,p) level. "TS" denotes transition state, "RC" denotes van der Waals pre-reaction complex and asterisk marks the TSs with hydrogen bonds.

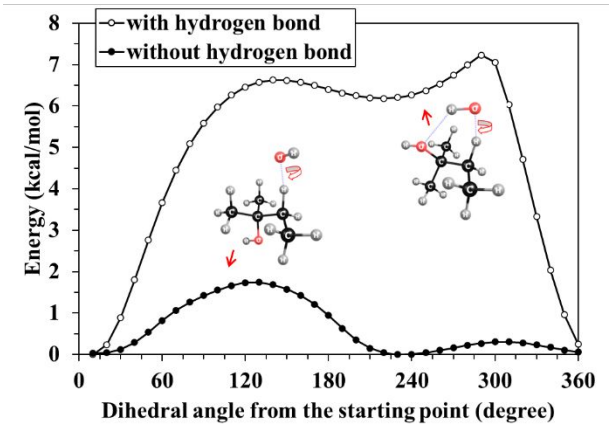

Fig. 3 Rotational potentials obtained at the M06-2X/6-31G level of theory for the same C–O torsional mode on the TS for s-β H-atom abstraction reaction channel with and without hydrogen bonds, respectively.

Table 2 The 47 normal mode vibrational frequencies (with those correspond to the six torsional modes removed) obtained at M06-2X/6-311++G(d,p) level of theory for the saddle point of s-β H-atom abstraction reaction channel with a hydrogen bond (ν) and without hydrogen bond (ν').

ν (cm^{-1}) (TS of s-β, with hydrogen bond)	ν' (cm^{-1}) (TS of s-β, without hydrogen bond)
138.44, 195.69, 257.57, 320.72, 369.66, 410.94,	83.77, 145.27, 257.73, 328.59, 372.53, 415.27,
462.23, 531.36, 680.33, 747.76, 877.41, 910.92,	450.33, 524.77, 657.80, 749.87, 774.63, 908.52,
939.45, 969.25, 1003.16, 1014.73, 1032.38,	940.16, 980.00, 1008.09, 1049.54, 1059.02,
1094.77, 1150.76, 1164.99, 1192.80, 1239.03,	1097.34, 1162.71, 1206.88, 1239.68, 1293.74,
1284.51, 1325.90, 1395.97, 1400.43, 1412.12,	1338.85, 1350.73, 1390.79, 1403.36, 1412.51,
1418.66, 1483.74, 1485.20, 1496.63, 1499.37,	1420.58, 1484.17, 1488.91, 1493.45, 1500.50,
1505.06, 1519.59, 1556.88, 3052.74, 3056.79,	1507.88, 1520.87, 1549.55, 3052.56, 3057.36,
3059.26, 3097.61, 3123.36, 3127.87, 3130.20,	3061.38, 3095.79, 3125.03, 3130.07, 3133.09,
3149.47, 3152.26, 3154.05, 3751.05, 3889.20	3138.97, 3146.41, 3153.07, 3799.67, 3882.43

VTST calculations were carried out for all H-atom abstraction reactions by ȮH. The minimum rate

coefficients were determined variationally based on a number of transition state structures along the reaction coordinate (defined by the distance between the O atom in the ȮH radical and the H atom being abstracted) obtained from the IRC calculations, at an energy-resolved level. The minimum energy paths (MEP) employed for the H-atom abstraction reaction channels from the carbon sites are shown in Fig. 4. When the TS structures without a hydrogen bond were used, the MEPs for the reactions are shifted upward by ~2 kcal mol^{-1} in energy, which will decrease the rate coefficients especially at low temperatures. However, contributions from the internal C–C and C–O rotations and the normal mode vibrations (especially those below 1000 cm^{-1}) to the overall molecular partition functions of the TS also increase, which can significantly accelerate the rate constants at higher temperatures. The overall influence of the hydrogen bond formed in the TS on the calculated rate coefficients are determined by their counter-balancing at different temperatures.

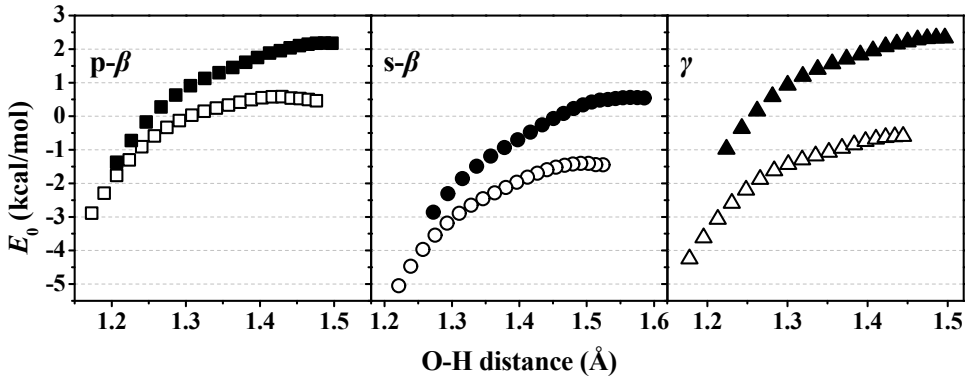

Fig. 4 ZPE corrected minimum energy paths obtained from IRC calculations at the M06-2X/6-311++G(d,p) level of theory for the H-atom abstraction reactions from the carbon sites of 2M2B. Solid symbols are electronic energies for the TS structures without hydrogen bond, while open symbols are those for TS structures with hydrogen bond.

Fig. 5 toFig. 7 show the calculated rate coefficients in this study for the p-β, s-β and γ H-atom abstraction reaction channels, respectively, in comparison with the reported rate coefficients in the literature for similar reaction pathways of other alcohol molecules. Note that the rate coefficients obtained in this study by using the TSs with a hydrogen bond and alternatively those without hydrogen bond are both shown. Since the TSs with a hydrogen bond all stay quite close to or below the reactants in energy, the corresponding rate coefficients exhibit a negative slope against temperature at temperatures below ~500 K. Moreover, the reaction kinetics is dominated by the energy barrier at lower temperatures, and the ratio of rate constants for the same reaction channel with/without a hydrogen bond in the TS can be 2–5 at 300 K. Whereas at temperatures above 500 K, the effects of energy barrier start to be overtaken by the effects of partition functions, and rate coefficients calculated by employing the TS without hydrogen bond become ~2 times higher. In terms of site-specific reaction kinetics, our calculated rate coefficients for 2M2B based on the TS structures without hydrogen bond are found to be more consistent with those for similar reaction pathways of 1-butanol,[48] 2-butanol,[49, 50] tert-butanol[51] and 3-methyl-1-butanol (3M1B)[20] at temperatures above 500 K.

View Article Online
DOI: 10.1039/D2CP02164A

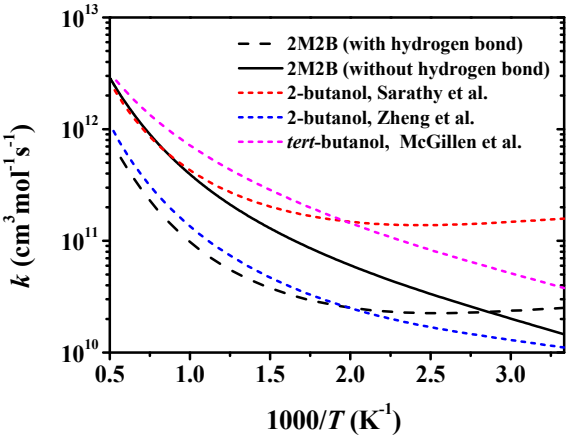

Fig. 5 Rate coefficients (per hydrogen atom) for the p-β H-atom abstraction reaction channel of 2M2B calculated in this study, 2-butanol from Sarathy et al.,[49] and Zheng et al.,[50] and *tert*-butanol from McGillen et al.,[51] respectively.

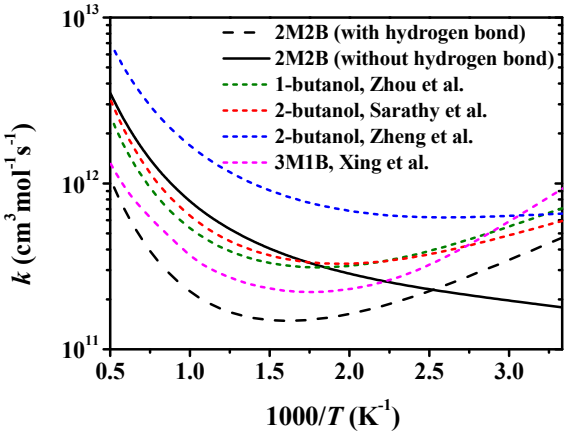

Fig. 6 Rate coefficients (per hydrogen atom) for the s-β H-atom abstraction reaction channel of 2M2B calculated in this study, 1-butanol from Zhou et al.,[48] 2-butanol from Zheng et al.[50] and Sarathy et al.,[49] and 3-methyl-1-butanol (3M1B) from Xing et al.,[20] respectively.

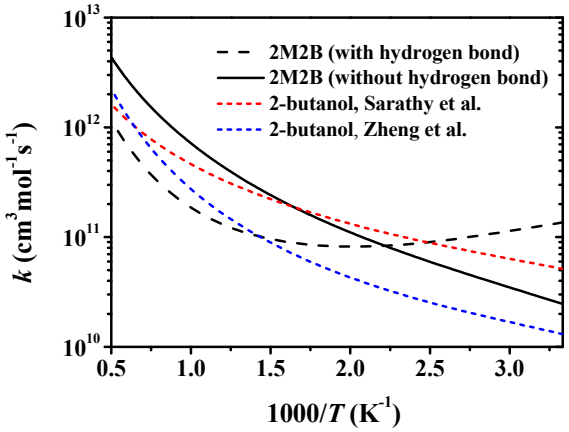

Fig. 7 Rate coefficients (per hydrogen atom) for the γ H-atom abstraction reaction channel of 2M2B calculated in this study, and 2-butanol from Sarathy et al.,[49] and Zheng et al.,[50] respectively.

The calculated rate coefficients for all H-atom abstraction reactions of 2M2B by ȮH and their branching ratios are shown in Fig. 8. The s-β H-atom abstraction reaction channel forming 2M2B-3-yl is the most

important at temperatures below 700 K because of its lowest energy barrier. While at temperatures of 1000 K or higher, the p-β and γ H-atom abstraction reaction pathways forming 2M2B-1-yl and 2M2B-4-yl, respectively are more competitive, with the first pathway being slightly faster. Abstraction of the hydrogen atom from the hydroxyl group by ȮH is the slowest throughout 300–2000 K and the formation of 2-methyl-2-butoxy is marginal. When employing the TS structures without hydrogen bond for the H-atom abstraction reaction pathways from the carbon sites, the relative importance of the p-β and γ H-atom abstraction reaction channels are slightly enhanced at temperatures above 1000 K and the ratio to hydroxyl group channel becomes negligible.

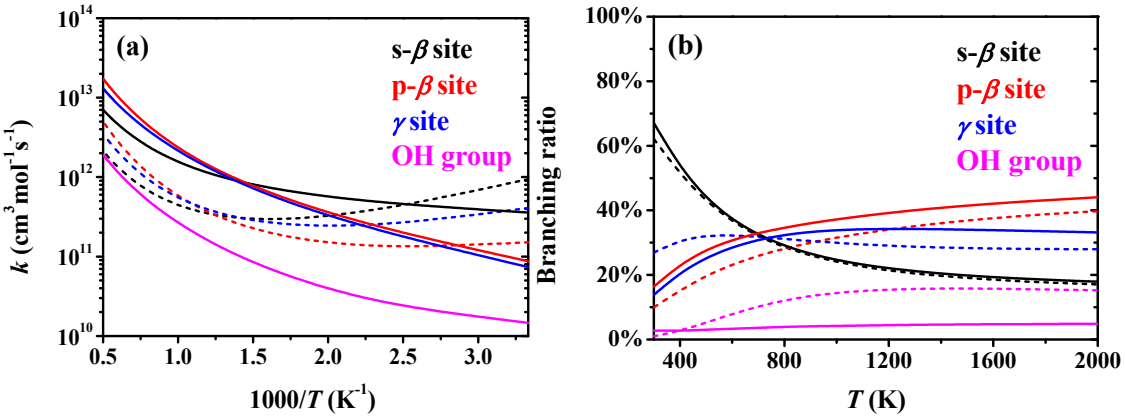

Fig. 8 (a) Rate coefficients for H-atom abstraction reactions of 2M2B and the corresponding (b) Branching ratios. Solid lines are the results obtained by employing TS structures without hydrogen bond, while dashed lines are the results for TS structures with hydrogen bond.

3.2. H_2O elimination reactions

2M2B molecule can undergo two different dehydration reaction pathways forming 2-methyl-1-butene and 2-methyl-2-butene, with energy barriers of 62.4 and 64.0 kcal mol^{-1}, respectively. The calculated energy barriers for the dehydration reactions of 2M2B are in good agreement with the average value, 62.4 kcal mol^{-1}, derived for this reaction class from a series of C_2–C_4 alcohols by Carstensen and Dean.[52] Given that the number of p-β H atoms is three times of the number of s-β H atoms, the formation of 2-methyl-1-butene + H_2O is faster than that of 2-methyl-2-butene + H_2O at various temperatures and pressures.

3.3. Isomerization and β-scission reactions of 2M2B radicals

The ZPE corrected PESs calculated at the QCISD(T)/CBS//M06-2X/6-311++G(d,p) level of theory for the unimolecular isomerization and β-scission reactions of the four 2M2B radicals, 2-methyl-2-butoxy (W1), 2M2B-1-yl (W2), 2M2B-3-yl (W3) and 2M2B-4-yl (W4), are shown in Fig. 9. For 2M2B-1-yl and 2M2B-3-yl, the C–O bond breaking will proceed through a TS with lower electronic energy than the products of alkene + ȮH. Hence, a van der Waals product complex was located for each of them, and variational corrections were employed for their TSs. The β C–C bond decomposition reaction of 2M2B-3-yl can proceed through two distinct TSs and form *trans*- and *cis*-2-buten-2-ol + $\dot{C}H_3$ (P6), respectively. They were considered as separate reaction channels in our calculations, with the energy barrier for the *cis* TS 0.8 kcal mol^{-1} higher. For 2-methyl-2-butoxy, the β-scission reaction pathways are predominantly favoured because of their significantly lower energy barriers compared with those of

isomerization pathways. The formations of 2-methyl-1-butene + ȮH and 2-methyl-2-butene + ȮH are energetically favoured for 2M2B-1-yl and 2M2B-3-yl, respectively. For 2M2B-4-yl, the β C–C bond breaking to form 2-hydroxyl-2-propyl + ethylene has the lowest energy barrier. Although the energy barriers for the isomerization channels through a five-membered ring TS, 2-methyl-2-butoxy ↔ 2M2B-4-yl and 2M2B-1-yl ↔ 2M2B-4-yl, are relatively low, these reaction channels are expected to be less important at high temperatures because of the entropy cost associated with the ring formed in the TS.

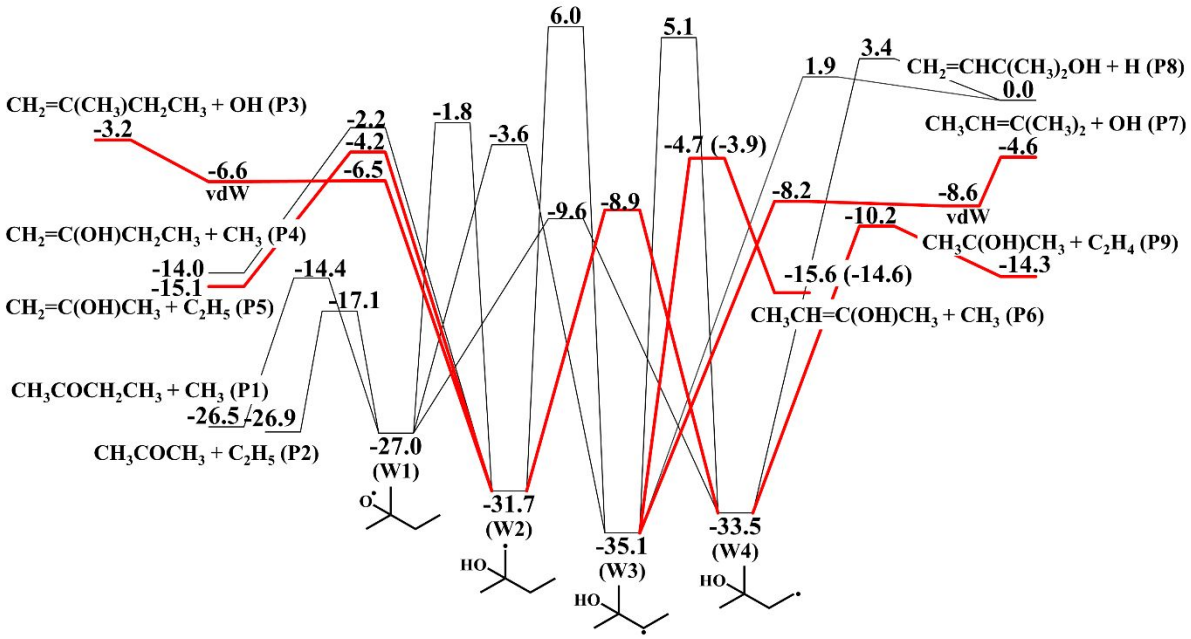

Fig. 9 ZPE corrected PESs (in units of kcal mol^{-1}) for the unimolecular isomerization and β-scission reactions of 2M2B radicals at the QCISD(T)/CBS//M06-2X/6-311++G(d,p) level (with important reaction channels in red). The relative energies for W3 = P6 (*cis*) are in parentheses.

For 2-methyl-2-butoxy, the β-scission reactions dominated over the entire temperature range from 300 to 2000 K, consistent with their considerably lower energy barriers, with the formations of acetone + ethyl (P2) and 2-butanone + methyl (P1) competing with each other. The calculated rate coefficients for the unimolecular reactions of 2M2B-1-yl as well as the product branching ratios at 1 and 10 atm are shown in Fig. 10. At temperatures below 600 K, 2M2B-1-yl predominantly isomerize to 2M2B-4-yl, because of the lower energy barrier of 22.8 kcal mol^{-1}, while at higher temperatures, the β-scission reactions of 2M2B-1-yl producing 2-methyl-1-butene + ȮH (P3) and propen-2-ol + $\dot{C}_2H_5$ (P5) become more competitive. When pressure elevates from 1 to 10 atm, the relative yield of 1-buten-2-ol + $\dot{C}H_3$ (P4) is slightly enhanced.

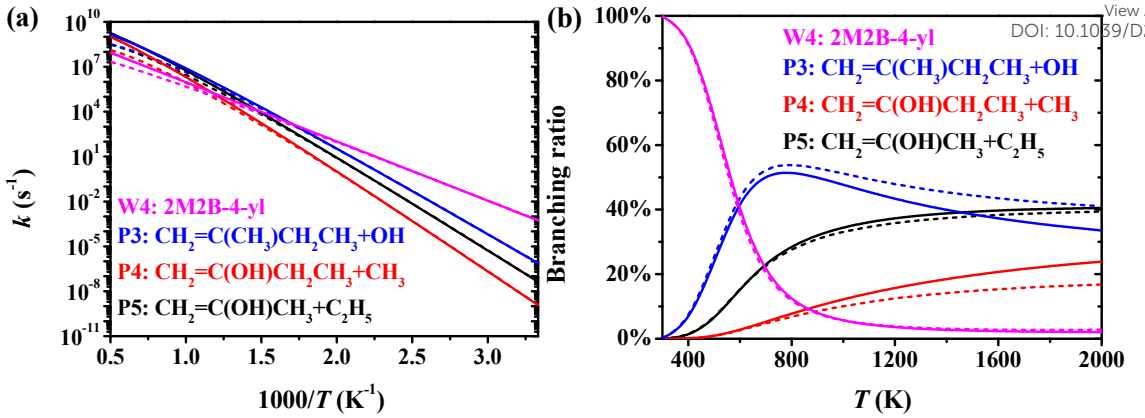

Fig. 10 Pressure-dependent (a) rate coefficients and (b) product branching ratios for the unimolecular reactions of 2M2B-1-yl (W2). Solid lines: 10 atm, dashed lines: 1 atm.

For the unimolecular reactions of 2M2B-3-yl, as illustrated in Fig. 11, the main products are *trans*- and *cis*-2-buten-2-ol + $\dot{C}H_3$ (P6) and 2-methyl-2-butene + $\dot{O}H$ (P7), while the formation of 2-methyl-3-buten-2-ol + $\dot{H}$ (P8) is negligible because of the pronouncedly higher energy barrier. The formation of 2-methyl-2-butene + $\dot{O}H$ dominates at temperatures below 1200 K, while the formation of 2-buten-2-ol + $\dot{C}H_3$ shows some significance at 1500 K and above. At higher pressures the relative importance of production shifts slightly from 2-methyl-2-butene + $\dot{O}H$ to 2-buten-2-ol + $\dot{C}H_3$ at high temperatures.

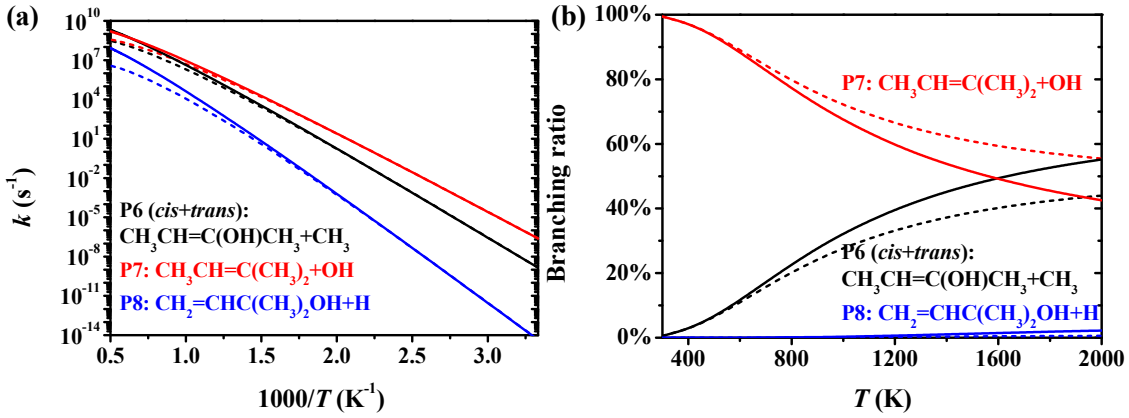

Fig. 11 Pressure-dependent (a) rate coefficients and (b) product branching ratios for the unimolecular reactions of 2M2B-3-yl (W3). Solid lines: 10 atm, dashed lines: 1 atm.

2M2B-4-yl almost completely decomposes to 2-hydroxyl-2-propyl + ethylene (P9) under combustion relevant temperatures and pressures. The calculated pressure-dependent rate coefficients for the formation of 2-hydroxyl-2-propyl + ethylene are shown in Fig. 12. Similar to the rate coefficients for the other β-scission reactions investigated here, the pressure fall-off effect of the kinetics of this reaction channel is more pronounced at pressures below 1 atm and temperatures above 500 K.

View Article Online
DOI: 10.1039/D2CP02164A

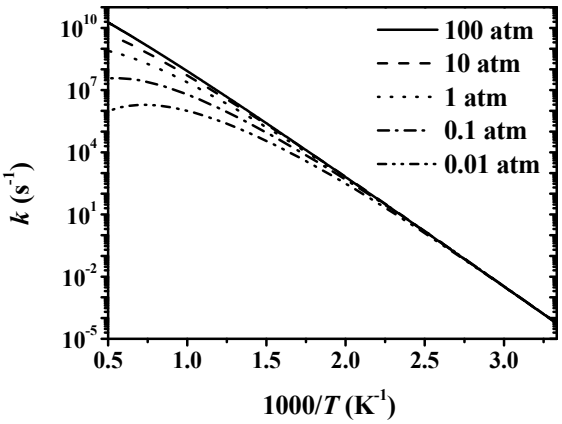

Fig. 12 Pressure-dependent rate coefficients for 2M2B-4-yl (W4) = $CH_3C(OH)CH_3$ + C_2H_4 (P9).

3.4. Thermochemistry

The calculated enthalpies of formation ($\Delta_f H^{\Theta}_{298}$) and entropies ($S^{\Theta}_{298}$) at standard conditions are shown in Table 3, compared with the available data from the Active Thermochemical Tables (ATcT),[53] the NIST Chemistry Webbook[54] and the Third Millennium Ideal Gas and Condensed Phase Thermochemistry Database for Combustion (Burcat database).[55] While heat capacities (C_p) at various temperatures are shown in Table 4. The calculated standard formation enthalpies are in excellent agreement with the available benchmark values in ATcT, all within 0.2 kcal mol^{-1}. In general, the deviations between our standard formation enthalpy results with the available data in NIST and Burcat databases are no larger than 1.2 kcal mol^{-1}, except for the standard formation enthalpy of *trans*-2-buten-2-ol and *cis*-2-buten-2-ol. The formation enthalpy for *trans*- and *cis*-2-buten-2-ol in the NIST database was measured by Turecek et al.,[56] being ~5 kcal mol^{-1} lower than our calculated one. Moreover, the estimated value by using Benson's group additivity method reported in ref. [56] was –49.5 kcal mol^{-1}, which is also lower by 2.8 kcal mol^{-1}. On the other hand, the calculated entropies at 298 K are in reasonable agreements with the literature data. The calculated heat capacities also agree well with the available data in the literature, with maximum deviation of 1.4 cal mol^{-1} K^{-1} over temperatures from 300 to 1500 K.

Table 3. The calculated standard formation enthalpy ($\Delta_f H^{\Theta}_{298}$) and entropy ($S^{\Theta}_{298}$) for each species in title reactions with literature data.

Species	$\Delta_f H^{\Theta}_{298}$ [kcal mol^{-1}]		S^{Θ}_{298} [cal mol^{-1} K^{-1}]	
	This study	Literature	This study	Literature
2-Butanone (P11)	–57.0	–57.0 ± 0.2[a], –57.0 ± 0.2[b], –56.9[b], –57.0[c]	81.2	81.3[c]
Methyl (P12)	35.1	35.0[a], 34.8[b], 35.1 ± 0.2[b], 35.1[c]	46.7	46.4[b], 46.4[c]
Acetone (P21)	–51.8	–51.8 ± 0.1[a], –51.9 ± 0.1[b], –52.0 ± 0.2[b], –51.7[b]	70.6	
Ethyl (P22)	28.7	28.7 ± 0.1[a], 28.4 ± 0.5[b], 28.6 ± 0.1[c]	60.6	60.5[21], 58.1[c]
2-Methyl-1-butene (P31)	–8.5	–8.4 ± 0.2[b], –8.3[b], –8.7[c]	82.3	81.2[c]
Hydroxyl (P32)	9.1	9.0[a], 9.3[b], 8.9 ± 0.1[c]	43.8	43.9[b], 43.9[c]
1-Buten-2-ol (P41)	–45.2		78.7	
Propen-2-ol (P51)	–40.6		69.4	
trans-2-Buten-2-ol (P61)	–46.7	–51.1[b]	79.4	
cis-2-Buten-2-ol (P61)	–45.6	–50.7[b]	79.0	
2-Methyl-2-butene (P71)	–10.1	9.9 ± 0.2[b], 9.8[b], –10.2[c]	80.4	80.9[b]
2-Methyl-3-buten-2-ol (P81)	–49.2		85.8	
2-Hydroxyl-2-propyl (P91)	–23.8		76.8	
Ethylene (P92)	12.5	12.5[a], 12.5[b], 12.5 ± 0.1[b], 12.5[c]	52.3	52.4[b], 52.4[c]

View Article Online
DOI: 10.1039/D2CP02164A

2-Methyl-2-butoxy (W1)	–25.9		88.2	
2M2B-1-yl (W2)	–29.9		93.2	
2M2B-3-yl (W3)	–33.2		91.6	
2M2B-4-yl (W4)	–31.7		92.4	
2M2B	–79.9	–78.7[b]	89.9	86.7 ± 1.6[b]

a Active Thermochemical Tables (Branco Ruscic Argonne National Lab).[53]

b NIST Chemistry Webbook.[54]

c Third Millennium Ideal Gas and Condensed Phase Thermochemical Database for Combustion (Burcat).[55]

Table 4. The calculated heat capacity (C_P) comparison for each species in title reactions with literature data.

Species	$C_p(T)$ [cal mol^{-1} K^{-1}]						
	300	400	500	600	800	1000	1500
2-Butanone (P11)	24.4	29.2	33.7	37.9	44.8	50.1	58.5
	24.4[b]	29.7[b]	34.7[b]	39.0[b]	46.0[b]	51.1[b]	59.1[b]
	24.5[c]						
Methyl (P12)	9.6	10.2	10.9	11.6	12.8	13.9	16.1
	9.3[b]	10.1[b]	10.8[b]	11.5[b]	12.9[b]	14.1[b]	16.3[b]
	9.2[c]						
Acetone (P21)	17.4	21.3	25.1	28.6	34.0	38.1	44.5
	18.0[b]	22.0[b]	25.8[b]	29.2[b]	34.7[b]	38.7[b]	45.1[b]
Ethyl (P22)	12.2	14.6	17.0	19.2	22.6	25.4	29.9
	12.1[c]						
2-Methyl-1-butene (P31)	25.7	32.1	38.2	43.6	51.8	58.2	68.1
	26.4[b]	33.2[b]	39.4[b]	44.7[b]	53.2[b]	59.4[b]	69.1[b]
	26.2[c]						
Hydroxyl (P32)	7.2	7.1	7.0	7.0	7.1	7.2	7.7
	7.2[b]	7.1[b]	7.1[b]	7.1[b]	7.2[b]	7.3[b]	7.9[b]
	7.1[c]						
1-Buten-2-ol (P41)	25.1	31.5	37.0	41.4	47.5	52.0	59.3
Propen-2-ol (P51)	20.0	24.7	28.8	32.0	36.4	39.7	45.1
trans-2-Buten-2-ol (P61)	25.0	30.2	34.9	39.1	45.6	50.6	58.5
cis-2-Buten-2-ol (P61)	24.6	30.3	35.3	39.6	45.9	50.8	58.7
2-Methyl-2-butene (P71)	24.8	30.9	36.9	42.3	50.8	57.4	67.6
	25.2[b]	31.9[b]	38.1[b]	43.4[b]	52.1[b]	58.5[b]	68.6[b]
	25.1[c]						
2-Methyl-3-buten-2-ol (P81)	31.9	39.0	45.2	50.3	58.0	63.8	73.1
2-Hydroxyl-2-propyl (P91)	21.1	25.0	28.9	32.3	37.7	41.9	48.5
Ethylene (P92)	10.1	12.3	14.5	16.6	19.6	22.1	25.9
	10.3[b]	12.7[b]	14.9[b]	16.9[b]	20.0[b]	22.4[b]	26.3[b]
	10.3[c]						
2-Methyl-2-butoxy (W1)	31.8	39.4	46.1	52.0	60.8	67.5	78.0
2M2B-1-yl (W2)	34.0	41.2	47.5	52.9	61.1	67.3	77.3
2M2B-3-yl (W3)	35.4	42.1	47.8	52.7	60.7	66.9	77.0
2M2B-4-yl (W4)	33.3	40.5	47.1	52.7	61.0	67.3	77.3
2-Methyl-2-butanol	33.0	40.8	47.9	54.1	63.4	70.5	81.7
		41.1[b]	47.8[b]				

a Active Thermochemical Tables (Branco Ruscic Argonne National Lab).[53]

b NIST Chemistry Webbook.[54]

c Third Millennium Ideal Gas and Condensed Phase Thermochemical Database for Combustion (Burcat).[55]

View Article Online
DOI: 10.1039/D2CP02164A

4. Conclusions

The kinetics of the important oxidation reactions of 2-methyl-2-butanol (2M2B) were studied in this study by performing high-level ab initio calculations. Rate coefficients for H-atom abstraction reactions from the primary β (p-β), secondary β (s-β) and γ sites of 2M2B were obtained, by employing the transition state structures with and without hydrogen bond separately, to analyse the effect of hydrogen bond formation in TS on the reaction kinetics. Rate coefficients calculated by using the TS structures with hydrogen bond are higher at temperatures below ~400 K, because of the lower energy barrier; whereas under combustion relevant temperature regime, the rate coefficients obtained from the TSs without hydrogen bond are higher. The s-β H-atom abstraction reaction channel is dominant at temperatures below 700 K, while the p-β and γ H-atom abstraction reaction channels are more competitive at 1000 K and above. For all unimolecular reactions studied, pressure-dependent rate coefficients were obtained from the solution of RRKM/ME, and the important product channels for each 2M2B radical was identified through their branching ratios. Temperature-dependent thermochemistry data for all species involved in the title reactions were calculated, which are found to be in good agreement with available data in the literature.

Acknowledgements

The work at Beihang University was supported by the National Science and Technology Major Project (2017-III-0004-0028) and Sinopec Science and Technology Department. The computational resources for this work were provided by the High-performance computing centre (HPC) at Beihang University.

Reference

1 K. Kohse-Höinghaus, P. Oßwald, T. A. Cool, T. Kasper, N. Hansen, F. Qi, C. K. Westbrook and P. R. Westmoreland, *Angew. Chem., Int. Ed.*, 2010, **49**, 3572-3597.

2 S. M. Sarathy, P. Oßwald, N. Hansen and K. Kohse-Höinghaus, *Prog. Energy Combust. Sci.*, 2014, **44**, 40-102.

3 Y. Yang, J. Dec, N. Dronniou and B. Simmons, *SAE Int. J. Fuels Lubr.*, 2010, **3**, 725-741.

4 M. Lapuerta, R. García-Contreras, J. Campos-Fernández and M. P. Dorado, *Energy Fuels*, 2010, **24**, 4497-4502.

5 B. Rajesh Kumar and S. Saravanan, *Fuel*, 2016, **170**, 49-59.

6 Z.-H. Zhang and R. Balasubramanian, *Appl. Energy*, 2016, **163**, 71-80.

7 A. F. Cann and J. C. Liao, *Applied Microbiology and Biotechnology*, 2010, **85**, 893-899.

8 L. Cai, F. vom Lehn and H. Pitsch, *Energy Fuels*, 2021, **35**, 1890-1917.

9 K. A. Heufer, S. M. Sarathy, H. J. Curran, A. C. Davis, C. K. Westbrook and W. J. Pitz, *Energy Fuels*, 2012, **26**, 6678-6685.

10 C. Togbé, F. Halter, F. Foucher, C. Mounaim-Rousselle and P. Dagaut, *Proc. Combust. Inst.*, 2011, **33**, 367-374.

11 Z. Serinyel, C. Togbé, G. Dayma and P. Dagaut, *Combust. Flame*, 2014, **161**, 3003-3013.

12 G. Dayma, C. Togbé and P. Dagaut, *Energy Fuels*, 2011, **25**, 4986-4998.

13 M. Köhler, T. Kathrotia, P. Oßwald, M. L. Fischer-Tammer, K. Moshammer and U. Riedel, *Combust. Flame*, 2015, **162**, 3197-3209.

14 C. Cao, Y. Zhang, X. Zhang, J. Zou, F. Qi, Y. Li and J. Yang, *Fuel*, 2019, **257**, 116039.

15 Q. Li, C. Tang, Y. Cheng, L. Guan and Z. Huang, *Energy Fuels*, 2015, **29**, 5334-5348.

16 R. Jalain, J. Bonnety, G. Legros and A. Matynia, *Fuel*, 2022, **307**, 121793.

17 L. Zhao, L. Ye, F. Zhang and L. Zhang, *J. Phys. Chem. A*, 2012, **116**, 9238-9244.

18 B. Aazaad and S. Lakshmipathi, *Mol. Phys.*, 2018, **116**, 1153-1165.

19 R. Van de Vijver, K. M. Van Geem, G. B. Marin and J. Zádor, *Combust. Flame*, 2018, **196**, 500-514.

20 L. Xing, Z. Wang and D. G. Truhlar, *J. Am. Chem. Soc.*, 2019, **141**, 18531-18543.

21 J. Bai, Y. Zhu, C.-W. Zhou, G. Dayma, Z. Serinyel and P. Dagaut, *Proc. Combust. Inst.*, 2021, **38**, 823-832.

22 F.-Y. Bai, M.-Y. Chen, X.-H. Liu, S. Ni, Y.-Z. Tang, X.-M. Pan and Z. Zhao, *New J. Chem.*, 2021, **45**, 16543-16556.

23 Y. Zhao and D. G. Truhlar, *Theor. Chem. Acc.*, 2008, **120**, 215-241.

24 A. D. McLean and G. S. Chandler, *J. Chem. Phys.*, 1980, **72**, 5639.

25 C. Hampel, K. A. Peterson and H.-J. Werner, *Chem. Phys. Lett.*, 1992, **190**, 1-12.

26 T. H. Dunning, *J. Chem. Phys.*, 1989, **90**, 1007-1023.

27 R. A. Kendall, T. H. Dunning Jr and R. J. Harrison, *J. Chem. Phys.*, 1992, **96**, 6796-6806.

28 M. Head-Gordon, J. A. Pople and M. J. Frisch, *Chem. Phys. Lett.*, 1988, **153**, 503-506.

29 D. E. Woon and T. H. Dunning Jr, *J. Chem. Phys.*, 1993, **98**, 1358-1371.

30 P. Zhang, S. J. Klippenstein and C. K. Law, *J. Phys. Chem. A*, 2013, **117**, 1890-1906.

31 H.-J. Werner, P. J. Knowles, G. Knizia, et al., MOLPRO, version 2015.1, a package of ab initio programs, see http://www.molpro.net.

32 https://github.com/Auto-Mech [accessed 21.09.23].

33 Y. Georgievskii, J. A. Miller, M. P. Burke and S. J. Klippenstein, *J. Phys. Chem. A*, 2013, **117**,

View Article Online
DOI: 10.1039/D2CP02164A

12146-12154.
34 C. Eckart, *Phys. Rev.*, 1930, **35**, 1303.
35 F. M. Mourits and F. H. A. Rummens, *Can. J. Chem.*, 1977, **55**, 3007-3020.
36 S. J. Klippenstein and J. A. Miller, *J. Phys. Chem. A*, 2005, **109**, 4285-4295.
37 M. Keçeli, S. N. Elliott, Y.-P. Li, M. S. Johnson, C. Cavallotti, Y. Georgievskii, W. H. Green, M. Pelucchi, J. M. Wozniak, A. W. Jasper and S. J. Klippenstein, *Proc. Combust. Inst.*, 2019, **37**, 363-371.
38 J. W. Ochterski, G. A. Petersson and J. A. Montgomery, *J. Chem. Phys.*, 1996, **104**, 2598-2619.
39 J. A. Montgomery, M. J. Frisch, J. W. Ochterski and G. A. Petersson, *J. Chem. Phys.*, 2000, **112**, 6532-6542.
40 L. A. Curtiss, K. Raghavachari, P. C. Redfern, V. Rassolov and J. A. Pople, *J. Chem. Phys.*, 1998, **109**, 7764-7776.
41 L. A. Curtiss, P. C. Redfern and K. Raghavachari, *J. Chem. Phys.*, 2007, **126**, 084-108.
42 J. M. Simmie and K. P. Somers, *J. Phys. Chem. A*, 2015, **119**, 7235-7246.
43 B. J. McBride and S. D. Gordon, Computer program for calculating and fitting thermodynamic functions, 1992.
44 B. Rotavera and C. A. Taatjes, *Prog. Energy Combust. Sci.*, 2021, **86**, 100925.
45 C. W. Zhou, J. M. Simmie and H. J. Curran, *Int. J. Chem. Kinet.*, 2012, **44**, 155-164.
46 Y. Georgievskii and S. J. Klippenstein, *J. Phys. Chem. A*, 2007, **111**, 3802-3811.
47 S. Xu, R. Zhu and M.-C. Lin, *Int. J. Chem. Kinet.*, 2006, **38**, 322-326.
48 C.-W. Zhou, J. M. Simmie and H. J. Curran, *Combust. Flame*, 2011, **158**, 726-731.
49 S. M. Sarathy, S. Vranckx, K. Yasunaga, M. Mehl, P. Oßwald, W. K. Metcalfe, C. K. Westbrook, W. J. Pitz, K. Kohse-Höinghaus and R. X. Fernandes, *Combust. Flame*, 2012, **159**, 2028-2055.
50 J. Zheng, G. A. Oyedepo and D. G. Truhlar, *J. Phys. Chem. A*, 2015, **119**, 12182-12192.
51 M. R. McGillen, M. Baasandorj and J. B. Burkholder, *J. Phys. Chem. A*, 2013, **117**, 4636-4656.
52 H.-H. Carstensen and A. M. Dean, in *Computational modeling in lignocellulosic biofuel production*, ACS Publications, 2010, pp. 201-243.
53 B. Ruscic and D. H. Bross, Active Thermochemical Tables (ATcT) values based on ver. 1.122r of the Thermochemical Network, 2021.
54 C. E. Lemmon, M. McLinden, D. Friend and W. M. P. Linstrom, NIST Chemistry Webbook, NIST Standard Reference Database Number 69, National Institute of Standards and Technology: Gaithersburg, 2021.
55 A. Burcat, B. Ruscic, Chemistry and T. I. I. of Tech, Third millenium ideal gas and condensed phase thermochemical database for combustion (with update from active thermochemical tables), 2005.
56 F. Turecek, L. Brabec and J. Korvola, *J. Am. Chem. Soc.*, 1988, **110**, 7984-7990.